Generation of single entangled photon-phonon pairs via an atom-photon-phonon interaction

Xun-Wei Xu [1,*] Hai-Quan Shi,[2,1] Jie-Qiao Liao,[3] and Ai-Xi Chen[4,1,†]

[1]*Department of Applied Physics, East China Jiaotong University, Nanchang 330013, China*

[2]*School of Materials Science and Engineering, Nanchang University, Nanchang 330031, China*

[3]*Key Laboratory of Low-Dimensional Quantum Structures and Quantum Control of Ministry of Education, Department of Physics and Synergetic Innovation Center for Quantum Effects and Applications, Hunan Normal University, Changsha 410081, China*

[4]*Department of Physics, Zhejiang Sci-Tech University, Hangzhou 310018, China*

(Received 15 May 2019; published 4 November 2019)

Antibunching and entanglement play important roles in quantum information processing as antibunching is an essential ingredient for the production of single photons (phonons) and entanglement is a crucial resource for quantum communication and metrology. In this paper, we propose a atom-photon-phonon (tripartite) interaction in a hybrid cavity-atom-mechanics system, and show that both photon and phonon antibunching can be observed simultaneously under the resonant atomic driving. More importantly, the generated single photons and phonons are strongly correlated and entangled with each other, i.e., single entangled photon-phonon pairs are generated via the atom-photon-phonon interaction. The generation of single entangled photon-phonon pairs is the first step to implement entanglement-based quantum state transfer, which is essential for connecting mechanical and optical systems to build hybrid quantum networks.

DOI: 10.1103/PhysRevA.100.053802

I. INTRODUCTION

Optomechanical systems with parametric coupling between optical and mechanical modes provide us a promising platform for generating and manipulating nonclassical photons and phonons [1]. As an important application, single-photon (-phonon) generation [2–4] in the optical (mechanical) mode based on optomechanical interaction has attracted significant interest in the past few years. A number of designs based on diverse mechanisms are proposed to demonstrate photon (phonon) antibunching in optomechanical systems, such as photon (phonon) antibunching based on strong optomechanical couplings [5–15] and photon (phonon) antibunching in the weak nonlinear regime induced by quantum interference [16–20].

In a recent experiment [21], the nonclassical correlation between single photons and phonons was reported by driving the nanomechanical photonic crystal cavity with a blue-detuned optical pulse. Additionally, quantum correlations between photons and phonons were also proposed theoretically based on indirect coupling via a two-level quantum dot [22]. Moreover, we studied the photon and phonon statistics in a quadratically coupled optomechanical system, and show that both photon and phonon antibunching can be observed in the same parameter regime and, more important, the single photons and single phonons are strongly anticorrelated [23]. Here, we will do a further study and propose a method to generate correlated single photons and phonons under constant atomic driving. Even more interestingly, we will show theoretically that the correlated single photons and phonons are entangled with each other, i.e., they are single entangled photon-phonon pairs.

Entangled states have great significance in both fundamental physics study and applications in quantum communication and metrology. Optomechanical entanglement has already been proposed theoretically [24–29] and demonstrated experimentally [30–33]. Both bipartite [34–37] and multipartite [38–42] entanglement have been proposed to be generated via optomechanical interaction. However, there are substantial differences between the entanglement we will discuss in this paper and the entanglement proposed previously. One striking difference is that the entanglement we propose here is for single photons and phonons, which are non-Gaussian, so that the generally adopted method, i.e., the linearization of the optomechanical interaction, is no longer applicable.

Inspired by a recent experiment [43], which presented a design of hybrid optomechanics by a quantum two-level system (qubit), here we consider a hybrid cavity-atom-mechanics system which enables a tripartite interaction between a two-level atom, an optical (or microwave) mode, and a mechanical mode. We note that a similar atom-photon-phonon interaction has been proposed in Refs. [44,45], and the tripartite interaction provides an optically controllable interaction between a two-level atom and a macroscopic mechanical oscillator by driving the optical mode strongly [19,45]. Nevertheless, in this paper, we will show that the atom-photon-phonon interactions with coherent atom driving can be used to generate single entangled photon-phonon pairs. As a crucial resource for quantum communication, single entangled photon-phonon pairs are essential for quantum state transfer by quantum teleportation, and the hybrid cavity-atom-mechanics system can serve as a quantum transducer in building hybrid quantum networks.

The remainder of this paper is organized as follows. In Sec. II, we introduce the theoretical model of a hybrid

*davidxu0816@163.com

†aixichen@zstu.edu.cn

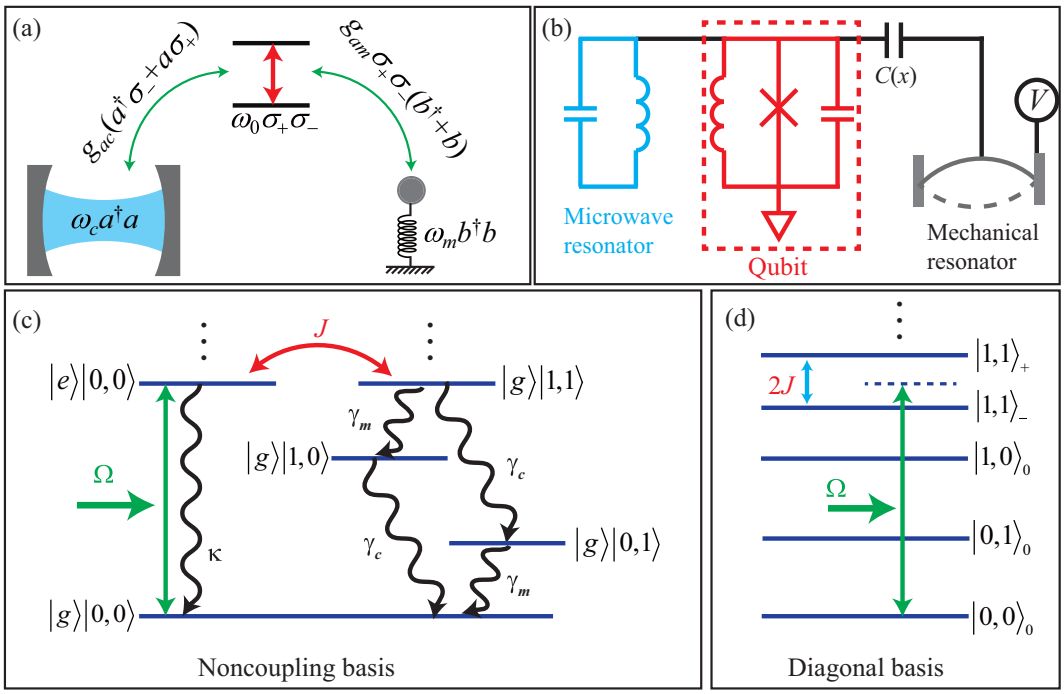

FIG. 1. (a) Schematic of a hybrid cavity-atom-mechanics system. (b) Electrical circuit scheme of the cavity-atom-mechanics tripartite system. (c, d) The energy spectrum of the hybrid system with atom-photon-phonon interaction [see the Hamiltonian in Eq. (5)] given (c) in the noncoupling basis and (d) in the diagonal basis.

cavity-atom-mechanics system, and show the simple derivation of the atom-photon-phonon interaction and the energy spectrum of the Hamiltonian. In Sec. III, the photon and phonon statistics, and the quantum correlation between the photons and phonons, are discussed numerically. Finally, a summary is given in Sec. IV.

II. MODEL AND HAMILTONIAN

We consider a hybrid cavity-atom-mechanics system, illustrated in Fig. 1(a), consisting of a two-level atom ($\sigma_\pm$ being the ladder operators) of transition frequency ω_0 coupling to an optical cavity a of resonance frequency ω_c with a transverse interaction $g_{ac}(a^\dagger + a)(\sigma_+ + \sigma_-)$, and coupling to a mechanical resonator b of resonance frequency ω_m with a longitudinal interaction $g_{am}\sigma_+\sigma_-(b^\dagger + b)$. A Hamiltonian of this kind has been realized in superconducting Josephson-junction quantum circuits [43] [see Fig. 1(b)], where a qubit (two-level system) is coupled to a microwave resonator with a transverse interaction $g_{ac}(a^\dagger + a)(\sigma_+ + \sigma_-)$, and a mechanical resonator is coupled to the qubit through a movable capacitance $C(x)$, which creates a longitudinal coupling $g_{am}\sigma_+\sigma_-(b^\dagger + b)$. It is worth mentioning that the optomechanical interaction $g_{om}a^\dagger a(b^\dagger + b)$ is ignored here as the coupling strength is weak, i.e., $g_{om} \ll \min\{g_{ac}, g_{am}\}$ [43,46]. Under the conditions $\max\{g_{ac}, g_{am}\} \ll \min\{\omega_0, \omega_c, \omega_m\}$, the hybrid system is described by the Hamiltonian under the rotating-wave approximation as ($\hbar = 1$)

$$\begin{aligned} H_{\rm hybrid} &= \omega_0\sigma_+\sigma_- + \omega_c a^\dagger a + \omega_m b^\dagger b \\ &\quad + g_{ac}(\sigma_+ a + a^\dagger\sigma_-) + g_{am}\sigma_+\sigma_-(b^\dagger + b) \\ &\quad + \Omega(\sigma_+ e^{-i\omega_p t} + \sigma_- e^{i\omega_p t}), \end{aligned} \tag{1}$$

where the two-level atom is pumped by a coherent field with strength Ω and frequency ω_p. By applying a displacement transformation $U \equiv \exp[\eta\sigma_+\sigma_-(b^\dagger - b)]$ with Lamb-Dicke parameter $\eta \equiv g_{am}/\omega_m$ to Eq. (1), we obtain the effective Hamiltonian $\widetilde{H} = U H_{\rm hybrid} U^\dagger$ as

$$\begin{aligned} \widetilde{H} &= \omega_0'\sigma_+\sigma_- + \omega_c a^\dagger a + \omega_m b^\dagger b \\ &\quad + g_{ac}[a\sigma_+ e^{\eta(b^\dagger - b)} + a^\dagger\sigma_- e^{-\eta(b^\dagger - b)}] \\ &\quad + \Omega[\sigma_+ e^{\eta(b^\dagger - b)} e^{-i\omega_p t} + \text{H.c.}], \end{aligned} \tag{2}$$

where $\omega_0' \equiv \omega_0 - \delta$ is the effective atomic transition frequency with frequency shift $\delta \equiv g_{am}^2/\omega_m$ induced by the displacement transformation.

Typically the coupling strength g_{am} is much smaller than the mechanical frequency ω_m, i.e., $\eta \ll 1$, so that $e^{\eta(b^\dagger - b)} \approx 1 + \eta(b^\dagger - b)$. Then we have

$$\begin{aligned} \widetilde{H} &\approx \omega_0'\sigma_+\sigma_- + \omega_c a^\dagger a + \omega_m b^\dagger b + g_{ac}(a\sigma_+ + a^\dagger\sigma_-) \\ &\quad + J(a\sigma_+ - a^\dagger\sigma_-)(b^\dagger - b) \\ &\quad + \Omega\{\sigma_+[1 + \eta(b^\dagger - b)]e^{-i\omega_p t} + \text{H.c.}\} \end{aligned} \tag{3}$$

where $J \equiv g_{ac}g_{am}/\omega_m$ is the tripartite atom-photon-phonon interaction strength. Under the conditions $\omega_0' = \omega_c + \omega_m$ and $\omega_p \approx \omega_0' > \{\omega_c, \omega_m\} \gg g_{ac} \gg \Omega$, the bipartite atom-photon interaction $g_{ac}(a\sigma_+ + a^\dagger\sigma_-)$ and sideband driving terms $\Omega[\sigma_+\eta(b^\dagger - b)e^{-i\omega_p t} + \text{H.c.}]$ can be ignored for large detuning. The remaining resonant interaction in the hybrid system is only the tripartite atom-photon-phonon interaction

$$H_{\rm int} = -J(\sigma_+ ab + \sigma_- a^\dagger b^\dagger), \tag{4}$$

which describes the simultaneous generation of a photon and a phonon with the two-level atom jumping from the excited state to its ground state and the reverse process.

We note that a similar tripartite interaction termed *mode field coupling* has been proposed theoretically in a multimode optomechanical system coupled to a two-level atom [45], which can be demonstrated experimentally by employing copper-doped silicon nanobeam optomechanical resonators [47]. Also, such interaction can be implemented in the electromechanical systems [30,48–50] with artificial atoms or in a Fabry-Pérot cavity with a membrane containing two-level atoms [51–54].

The effective Hamiltonian for the hybrid cavity-atom-mechanics system in the rotating frame with respect to $R(t) = \exp[i\omega_p\sigma_+\sigma_- t + i(\omega_p - \omega_m)a^\dagger a t + i\omega_m b^\dagger b t]$ reads

$$H_{\rm eff} = \Delta\sigma_+\sigma_- + \Delta a^\dagger a - J(\sigma_+ ab + \sigma_- a^\dagger b^\dagger) + \Omega\sigma_x, \quad (5)$$

where we introduce the detuning $\Delta \equiv \omega_0' - \omega_p = \omega_c + \omega_m - \omega_p \ll \omega_m$. This hybrid cavity-atom-mechanics system with tripartite atom-photon-phonon interaction provides us an effective way to generate photon-phonon pairs. The validity of the effective Hamiltonian has been checked numerically in the Appendix. Numerical examples illustrate that almost the same results can be obtained by the Hamiltonian in Eq. (1) and the effective Hamiltonian in Eq. (5) under the conditions $\omega_0' = \omega_c + \omega_m$ and $\omega_p \approx \omega_0' > \{\omega_c, \omega_m\} \gg \{g_{ac}, g_{am}\} \gg \Omega$.

The energy spectrum of the effective Hamiltonian in Eq. (5) for the hybrid cavity-atom-mechanics system is shown in Figs. 1(c) and 1(d). In the noncoupling basis [Fig. 1(c)], $|e\rangle$ ($|g\rangle$) denotes the excited (ground) state of the two-level atom, and $|n, m\rangle$ represents the Fock state with n photons in the optical mode and m phonons in the mechanical mode. In Fig. 1(d), we denote the eigenstates in the diagonal basis as $|0, 0\rangle_0 \equiv |g\rangle|0, 0\rangle$, $|1, 0\rangle_0 \equiv |g\rangle|1, 0\rangle$, $|0, 1\rangle_0 \equiv |g\rangle|0, 1\rangle$, and $|1, 1\rangle_\pm \equiv (|g\rangle|1, 1\rangle \pm |e\rangle|0, 0\rangle)/\sqrt{2}$ with eigenvalues zero, ω_c, ω_m, and $\omega_0' \pm J$, respectively.

III. CORRELATION AND ENTANGLEMENT

To quantify the statistics of the phonons and photons in the system, we consider the equal-time second-order correlation functions $g_n^{(2)}(0)$ and $g_m^{(2)}(0)$ and cross-correlation function $g_{nm}^{(2)}(0)$ in the steady state ($t \to \infty$) defined by

$$g_n^{(2)}(0) \equiv \frac{\langle a^\dagger a^\dagger a a\rangle}{\langle n\rangle^2}, \quad (6)$$

$$g_m^{(2)}(0) \equiv \frac{\langle b^\dagger b^\dagger b b\rangle}{\langle m\rangle^2}, \quad (7)$$

$$g_{nm}^{(2)}(0) \equiv \frac{\langle a^\dagger b^\dagger b a\rangle}{\langle n\rangle\langle m\rangle}, \quad (8)$$

where $\langle n\rangle \equiv \langle a^\dagger a\rangle$ and $\langle m\rangle \equiv \langle b^\dagger b\rangle$ are the mean photon and phonon numbers. The dynamic behavior of the total open system is described by the master equation for the density matrix ρ of the system [55]

$$\frac{\partial\rho}{\partial t} = -i[H_{\rm eff}, \rho] + \kappa L[\sigma_-]\rho + \gamma_c L[a]\rho + \gamma_m(m_{\rm th}+1)L[b]\rho + \gamma_m m_{\rm th} L[b^\dagger]\rho, \quad (9)$$

where $L[o]\rho = o\rho o^\dagger - (o^\dagger o\rho + \rho o^\dagger o)/2$ denotes a Lindblad term for an operator o; κ is the damping rate of the two-level atom and γ_c (γ_m) is the damping rate of the optical (mechanical) mode; $m_{\rm th}$ is the mean thermal phonon number. We assume that the frequencies of the two-level atom and the optical mode are so high that the thermal effect can be neglected.

The equal-time second-order correlation functions [$g_n^{(2)}(0)$ and $g_m^{(2)}(0)$] and cross-correlation function $g_{nm}^{(2)}(0)$ are plotted as functions of the detuning Δ/κ in Fig. 2 under both weak-coupling condition [(a) $J = 0.1\kappa$] and strong-coupling condition [(c) $J = 100\kappa$]. It is clear that both photon antibunching and phonon antibunching, i.e., $g_n^{(2)}(0) = g_m^{(2)}(0) < 1$, appear with the same optical and mechanical damping rates ($\gamma_c = \gamma_m = 10\kappa$). Moreover, the antibunching (single) photons and phonons are strongly correlated with each other, i.e., $g_{nm}^{(2)}(0) \gg 1$, which means that the single photons and phonons are generated simultaneously or in pairs. The optimal detuning Δ for generating single entangled photon-phonon pairs depends on the coupling strength J: $\Delta = 0$ for weak coupling and $|\Delta| \approx J$ for strong coupling. Moreover, the mean photon (phonon) number $\langle n\rangle = \langle m\rangle$ in the weak-coupling regime is much smaller than the one in the strong-coupling case.

Physically, the single entangled photon-phonon pairs are generated one by one with the two-level atom jumping from the excited state to its ground state. In the weak-coupling regime ($J \ll \kappa$), the system is driven resonantly with detuning $\Delta = 0$ because the states $|1, 1\rangle_+$ and $|1, 1\rangle_-$ are not resolved. In the strong-coupling regime ($J \gg \kappa$), the system should be investigated by the dressed states as shown in Fig. 1(d), and the single photon-phonon pairs are generated with detuning $\Delta = \pm J$ for resonant pumping.

In order to understand the behavior of the cross-correlation function $g_{nm}^{(2)}(0)$, we can give the expression of $g_{nm}^{(2)}(0)$ approximately. Under the weak-exciting condition, i.e., $\max\{\langle n\rangle, \langle m\rangle\} \ll 1$, we have mean photon (phonon) number

$$\langle n\rangle \approx \rho_{5,5} + \rho_{4,4}, \quad (10)$$

$$\langle m\rangle \approx \rho_{5,5} + \rho_{3,3}, \quad (11)$$

and the cross-correlation function $g_{nm}^{(2)}(0)$

$$g_{nm}^{(2)}(0) \approx \frac{\rho_{5,5}}{(\rho_{5,5} + \rho_{3,3})(\rho_{5,5} + \rho_{4,4})}, \quad (12)$$

where $\rho_{3,3} = \langle g|\langle 0, 1|\rho|g\rangle|0, 1\rangle$, $\rho_{4,4} = \langle g|\langle 1, 0|\rho|g\rangle|1, 0\rangle$, and $\rho_{5,5} = \langle g|\langle 1, 1|\rho|g\rangle|1, 1\rangle$, and they satisfy the relations

$$\rho_{3,3} \approx \frac{\gamma_c}{\gamma_m}\rho_{5,5}, \quad (13)$$

$$\rho_{4,4} \approx \frac{\gamma_m}{\gamma_c}\rho_{5,5}. \quad (14)$$

As we set $\gamma_c = \gamma_m$, then we have $\rho_{3,3} \approx \rho_{4,4} \approx \rho_{5,5}$, $\langle n\rangle = \langle m\rangle \approx 2\rho_{5,5}$, and

$$g_{nm}^{(2)}(0) \approx \frac{1}{2\langle n\rangle}. \quad (15)$$

Under the resonant conditions at the detuning $\Delta = 0$ for weak coupling and $|\Delta| \approx J$ for strong coupling, we have maximum $\langle n\rangle = \langle m\rangle$, and thus minimum cross-correlation function

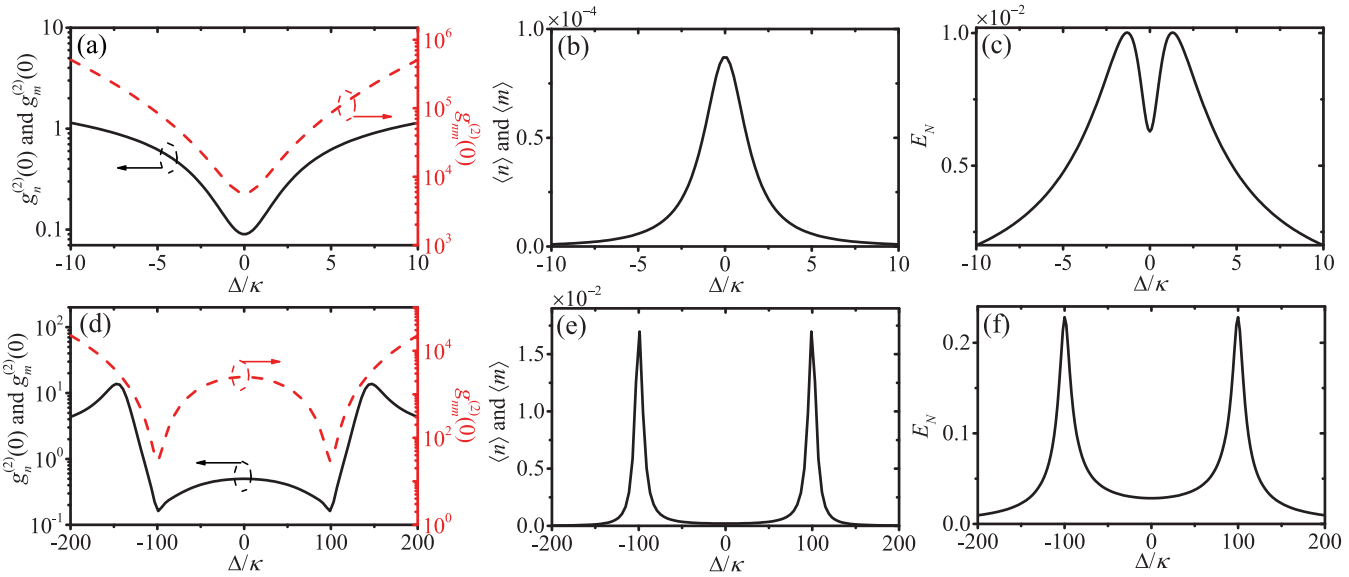

FIG. 2. In panels (a) and (d), the equal-time second-order correlation functions $[g_n^{(2)}(0)$ and $g_m^{(2)}(0)]$ and cross-correlation function $g_{nm}^{(2)}(0)$ are plotted as functions of the detuning Δ/κ. In panels (b) and (e), the mean photon (phonon) number $[\langle n\rangle = \langle m\rangle]$ is plotted as a function of the detuning Δ/κ. In panels (c) and (f), the logarithmic negativity E_N is plotted as a function of the detuning Δ/κ. We set $J = 0.1\kappa$ in panels (a)–(c) and set $J = 100\kappa$ in panels (d)–(f). Other used parameters are $\gamma_c = \gamma_m = 10\kappa$, $\Omega = \kappa$, and $m_{\rm th} = 0$.

$g_{nm}^{(2)}(0)$, corresponding to the dips around the detuning $\Delta = 0$ for weak coupling and $|\Delta| \approx J$ for strong coupling.

It is not hard to guess that the strongly correlated single photons and single phonons generated simultaneously are entangled with each other. The entanglement between the optical and mechanical modes can be characterized by the logarithmic negativity [56]

$$E_N = \log_2 \left\| \rho_{AB}^{T_A} \right\|_1, \tag{16}$$

where the symbol $\|\cdot\|_1$ denotes the trace norm, and $\rho_{AB}^{T_A}$ is the partial transpose of the reduced density matrix ρ_{AB} of the optical and mechanical modes. The logarithmic negativity E_N is non-negative and $E_N > 0$ would mean that the generated single photons and single phonons are entangled. It is worth mentioning that the entangled state for the single photons and single phonons obtained here is non-Gaussian. Thus the logarithmic negativity for Gaussian states [57] widely used in the previous works [24–29] cannot be used to accurately describe the entangled state here.

The logarithmic negativity E_N is shown in Figs. 2(c) and 2(f). Obviously, the strongly correlated single photons and single phonons generated simultaneously are entangled with each other in both the weak-coupling ($J < \kappa$) and strong-coupling ($J > \kappa$) regimes. In the weak-coupling regime as shown in Fig. 2(c), there is a dip around the detuning $\Delta = 0$, which is induced by the quantum interferences between two routes: (a) the direct transition channel $|g\rangle|0,0\rangle \xrightarrow{\Omega} |e\rangle|0,0\rangle \xrightarrow{J} |g\rangle|1,1\rangle$ and (b) the indirect transition channel $|g\rangle|0,0\rangle \xrightarrow{\Omega} |e\rangle|0,0\rangle \xrightarrow{\Omega} |g\rangle|0,0\rangle \xrightarrow{\Omega} |e\rangle|0,0\rangle \xrightarrow{J} |g\rangle|1,1\rangle$ (or higher-order variants). Thus the width of the dip depends on the driving strength Ω, as shown in Fig. 3(a). Similar mechanisms can induce transparency in lambda-type three-level atoms [58,59] and optomechanical systems [60–62]. Differently, in Fig. 2(f), there are two peaks around the detunings $\Delta = \pm J$ in the strong-coupling regime. This phenomenon can be understood by analyzing the energy spectrum shown in Fig. 1(d): the transition process $|0,0\rangle_0 \to |1,1\rangle_\pm$ is resonantly enhanced with detunings $\Delta = \pm J$. As a consequence, we can shift the optimal value of the detuning for entanglement by tuning the coupling strength J as shown in Fig. 3(b).

Figure 4 shows the second-order correlation functions $[g_n^{(2)}(0)$ and $g_m^{(2)}(0)]$ and cross-correlation function $g_{nm}^{(2)}(0)$ with the coupling strength J from weak to strong. The mean photon (phonon) number $[\langle n\rangle = \langle m\rangle]$ and logarithmic

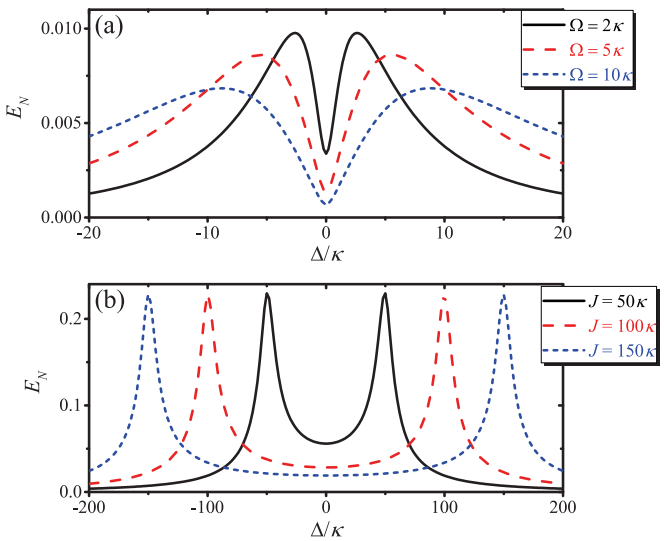

FIG. 3. The logarithmic negativity E_N is plotted as a function of the detuning Δ/κ for different driving strengths Ω in panel (a) and for different coupling strengths J in panel (b). We set $J = 0.1\kappa$ in panel (a) and set $\Omega = \kappa$ in panel (b). Other used parameters are $\gamma_c = \gamma_m = 10\kappa$ and $m_{\rm th} = 0$.

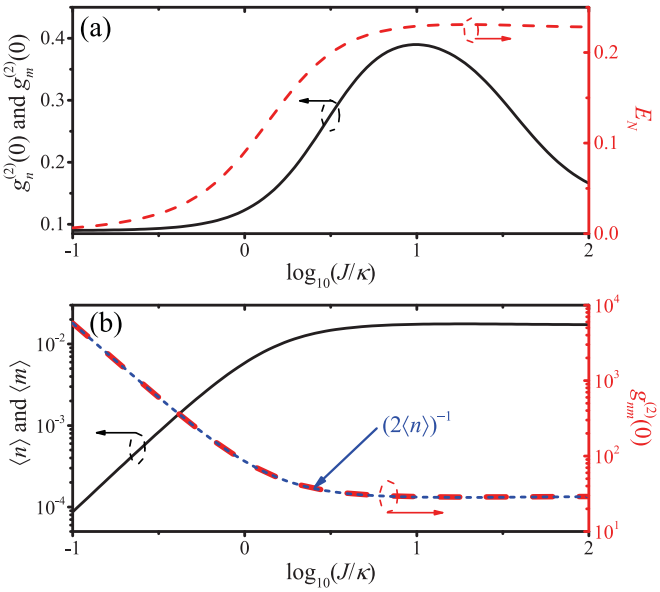

FIG. 4. (a) The equal-time second-order correlation functions $[g_n^{(2)}(0)$ and $g_m^{(2)}(0)]$ of the logarithmic negativity E_N are plotted as functions of the coupling strength $\log_{10}(J/\kappa)$. (b) The mean photon (phonon) number $[\langle n\rangle$ and $\langle m\rangle]$ and cross-correlation function $g_{nm}^{(2)}(0)$ are plotted as functions of $\log_{10}(J/\kappa)$. There are two curves for $g_{nm}^{(2)}(0)$, where the red dashed one is obtained from Eq. (9) and the blue short-dashed one is obtained from Eq. (15). Other used parameters are $|\Delta| = J$, $\gamma_c = \gamma_m = 10\kappa$, $\Omega = \kappa$, and $m_{\rm th} = 0$.

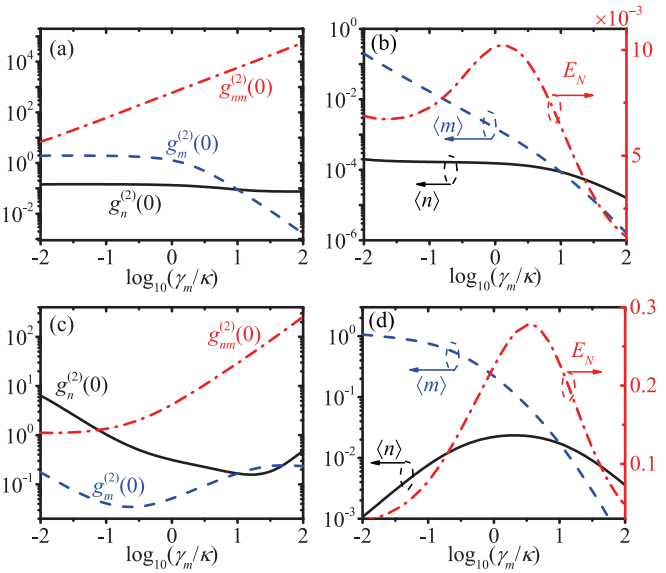

FIG. 5. (a, c) The equal-time second-order correlation functions $[g_n^{(2)}(0)$ and $g_m^{(2)}(0)]$ and cross-correlation function $g_{nm}^{(2)}(0)$ are plotted as functions of the mechanical damping rate $\log_{10}(\gamma_m/\kappa)$. (b, d) The mean photon (phonon) number $[\langle n\rangle$ and $\langle m\rangle]$ and the logarithmic negativity E_N are plotted as functions of the mechanical damping rate $\log_{10}(\gamma_m/\kappa)$. We set $J = 0.1\kappa$ in panels (a) and (b) and set $J = 100\kappa$ in panels (c) and (d). Other used parameters are $|\Delta| = J$, $\gamma_c = 10\kappa$, $\Omega = \kappa$, and $m_{\rm th} = 0$.

negativity E_N increase with the enhancing of the coupling strength J. As shown in Fig. 4(b), the cross-correlation function $g_{nm}^{(2)}(0)$ decreases with the increasing of the mean photon (phonon) number $[\langle n\rangle = \langle m\rangle]$, and the numerical results (red dashed curve) agree well with the analytical results given in Eq. (15) (blue short-dashed curve). The second-order correlation functions $[g_n^{(2)}(0)$ and $g_m^{(2)}(0)]$ increase first with the mean photon (phonon) number, and then decrease with the coupling strength J. The suitable coupling strength J for observing correlated single photons and single phonons, i.e., $g_n^{(2)}(0) = g_m^{(2)}(0) \ll 1$ and $g_{nm}^{(2)}(0) \gg 1$, is $J \ll \kappa$ or $J \gg \kappa$.

Generally, the damping rate of the mechanical mode is much smaller than the damping rate of the optical mode. However, the effective damping of the mechanical mode can be controlled and significantly enhanced by coupling the mechanical mode to an auxiliary optical mode [63–66]. In addition, the phonon statistics can be observed indirectly by measuring statistics of the photons output from the auxiliary optical mode [67–70]. The dependence of the second-order correlation functions $[g_n^{(2)}(0)$ and $g_m^{(2)}(0)]$ and cross-correlation function $g_{nm}^{(2)}(0)$ on the mechanical damping rate γ_m is shown in Fig. 5. In the weak-coupling case [Figs. 5(a) and 5(b)], the correlation and cross-correlation functions change monotonically with the mechanical damping rate. In the strong-coupling case [Figs. 5(c) and 5(d)], the correlation and cross-correlation functions change nonmonotonously with the mechanical damping rate. The mean phonon number $\langle m\rangle$ decreases rapidly with the mechanical damping rate in both weak- and strong-coupling regimes and the mean photon number $\langle n\rangle$ decreases monotonously for weak coupling ($J \ll \kappa$), while $\langle n\rangle$ increases first and then decreases with the mechanical damping rate in the strong-coupling regime ($J \gg \kappa$), i.e., we can enhance photon emission by increasing the mechanical damping rate when $\gamma_m < \kappa$. Moreover, there is an optimal mechanical damping rate γ_m for entanglement E_N around the point $\gamma_m \approx 1.32\kappa$ ($\gamma_m \approx 3.47\kappa$) in the case of $J = 0.1\kappa$ ($J = 100\kappa$).

These interesting phenomena can be understood by the probability distribution in the bare states as shown in Fig. 6, where $\rho_{1,1} = \langle g|\langle 0,0|\rho|g\rangle|0,0\rangle$, $\rho_{2,2} = \langle e|\langle 0,0|\rho|e\rangle|0,0\rangle$, $\rho_{3,3} = \langle g|\langle 0,1|\rho|g\rangle|0,1\rangle$, $\rho_{4,4} = \langle g|\langle 1,0|\rho|g\rangle|1,0\rangle$, $\rho_{5,5} = \langle g|\langle 1,1|\rho|g\rangle|1,1\rangle$, $\rho_{1,5} = \langle g|\langle 0,0|\rho|g\rangle|1,1\rangle$, and $\rho_{2,5} = \langle e|\langle 0,0|\rho|g\rangle|1,1\rangle$. It is clear that we have $\rho_{3,3} \approx \rho_{4,4} \approx \rho_{5,5}$ around $\gamma_m = \gamma_c$, which agrees with Eqs. (13) and (14). In the weak-coupling regime ($J \ll \kappa$) as shown in Fig. 6(a), most of the probability is distributed in the states $|g\rangle|0,0\rangle$ and $|e\rangle|0,0\rangle$; the probability in states $|g\rangle|1,1\rangle$ (as well as the off-diagonal elements $|\rho_{1,4}|$ and $|\rho_{1,5}|$, which determine the entanglement E_N between the photons and phonons) increases slowly in the regime of $\gamma_m < \kappa$, and decreases rapidly when $\gamma_m > \kappa$; the probability in single-phonon state $|g\rangle|0,1\rangle$ (single-photon state $|g\rangle|1,0\rangle$) decreases (increases) in the regime of $\gamma_m < \gamma_c$, and decreases rapidly when $\gamma_m > \gamma_c$. Differently, in the strong-coupling regime ($J \gg \kappa$) as shown in Fig. 6(b), most of the probability (87.5%) is distributed in the single-phonon state $|g\rangle|0,1\rangle$ when $\gamma_m \ll \kappa$, as the damping rate of the state $|g\rangle|0,1\rangle$ is much smaller than the other states; the probability in the ground state $|g\rangle|0,0\rangle$ increases monotonously with the mechanical damping rate; the probabilities in states $|e\rangle|0,0\rangle$ and $|g\rangle|1,1\rangle$ are almost the same, i.e., $\rho_{2,2} \approx \rho_{5,5}$, and they (as well as the off-diagonal

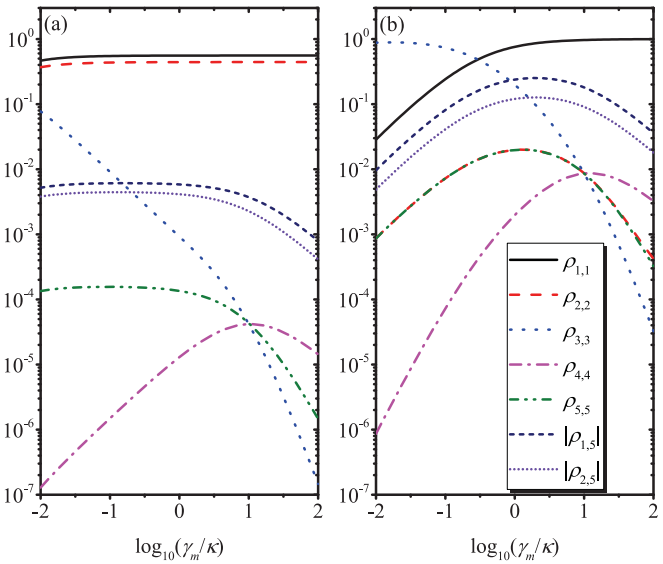

FIG. 6. The elements of the density matrix ρ from Eq. (9) in the steady state are plotted as functions of the mechanical damping rate $\log_{10}(\gamma_m/\kappa)$, where $\rho_{1,1} = \langle g|\langle 0,0|\rho|g\rangle|0,0\rangle$, $\rho_{2,2} = \langle e|\langle 0,0|\rho|e\rangle|0,0\rangle$, $\rho_{3,3} = \langle g|\langle 0,1|\rho|g\rangle|0,1\rangle$, $\rho_{4,4} = \langle g|\langle 1,0|\rho|g\rangle|1,0\rangle$, $\rho_{5,5} = \langle g|\langle 1,1|\rho|g\rangle|1,1\rangle$, $\rho_{1,5} = \langle g|\langle 0,0|\rho|g\rangle|1,1\rangle$, and $\rho_{2,5} = \langle e|\langle 0,0|\rho|g\rangle|1,1\rangle$. We set $J = 0.1\kappa$ in panel (a) and set $J = 100\kappa$ in panel (b). Other used parameters are $|\Delta| = J$, $\gamma_c = 10\kappa$, $\Omega = \kappa$, and $m_{\rm th} = 0$.

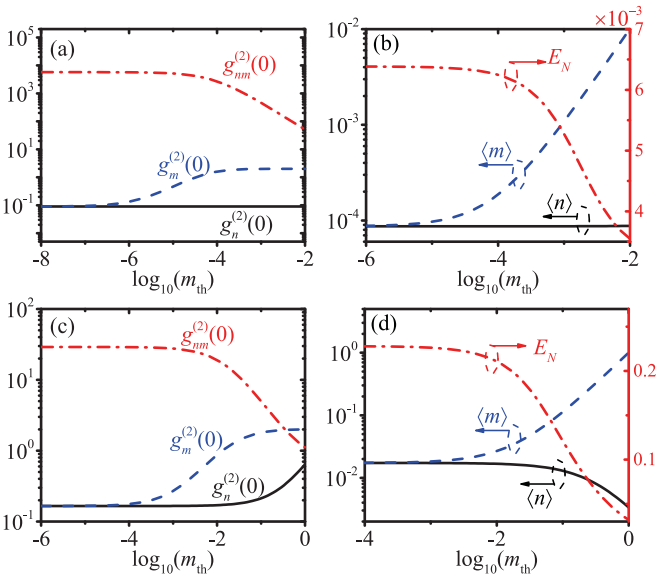

FIG. 7. (a, c) The equal-time second-order correlation functions $[g^{(2)}_n(0)$ and $g^{(2)}_m(0)]$ and cross-correlation function $g^{(2)}_{nm}(0)$ are plotted as functions of the mean thermal phonon number $\log_{10}(m_{\rm th})$. (b, d) The mean photon (phonon) number $[\langle n\rangle$ and $\langle m\rangle]$ and the logarithmic negativity E_N are plotted as functions of the mean thermal phonon number $\log_{10}(m_{\rm th})$. We set $J = 0.1\kappa$ in panels (a) and (b) and set $J = 100\kappa$ in panels (c) and (d). Other used parameters are $|\Delta| = J$, $\gamma_c = \gamma_m = 10\kappa$, and $\Omega = \kappa$.

elements $|\rho_{1,4}|$ and $|\rho_{1,5}|$) increase first and then decrease with the mechanical damping rate, corresponding to the phenomena of photon emission and entanglement enhancing by increasing the mechanical damping rate when $\gamma_m < \kappa$.

The thermal effect of the mechanical mode on the statistic properties of the generated photons and phonons is shown in Fig. 7. It is clear that the thermal phonons have a significant effect on the statistic properties of the generated photons and phonons. As the mean phonon number is much larger in the strong-coupling regime than the in the weak-coupling regime, the correlated and entangled single photons and phonons in the strong-coupling regime are more robust against thermal noise than those in the weak-coupling regime.

IV. CONCLUSIONS

In summary, we have proposed a scheme to generate single entangled photon-phonon pairs in a hybrid optomechanical system via atom-photon-phonon (tripartite) interaction. The single phonons with low loss can be used for quantum memories, and single photons are suitable quantum information carriers. The generation of single entangled photon-phonon pairs is the first step to implement entanglement-based quantum state transfer between quantum memories and optical communication channels, which is essential for building hybrid quantum networks.

The conditions required to generate single entangled photon-phonon pairs in a hybrid optomechanical system are $\omega_0 \gg \{\omega_c, \omega_m\} \gg \{g_{ac}, g_{am}\}$. One promising candidate for realizing our proposal is the cavity optomechanics in the microwave frequency regime involving a Josephson-junction qubit as shown in Ref. [43], with $\omega_0/2\pi \simeq 5$–10 GHz, $\omega_c/2\pi \simeq 5$ GHz, $g_{ac}/2\pi \simeq 0$–500 MHz, and $g_{am}/2\pi \simeq 80$–160 MHz, except the mechanical frequency $\omega_m/2\pi \simeq 65$ MHz, which still needs to be improved by several orders of magnitude for our proposal. We note that the fabrication of gigahertz-frequency mechanical oscillators can be achieved with the current state of the art. For example, a mechanical resonator with frequency as high as 6 GHz coupled to a superconducting qubit on a single chip has been applied to measure the quantum state of the resonator [71]. Thus our proposal should be feasible for experiments. In addition, the basic mechanism of this paper can be generalized to a nondegenerate two-photon Jaynes-Cummings model [72,73], to generate entangled photon pairs with different frequency, such as entangled microwave-optical photon pairs [74], and shed new light on quantum state transfer between electromagnetic modes with different frequencies.

ACKNOWLEDGMENTS

We thank Y.-J. Zhao, H. Wang, and Q. Zheng for helpful discussions. X.-W.X. was supported by the National Natural Science Foundation of China (NSFC) under Grant No. 11604096 and by the Key Program of Natural Science Foundation of Jiangxi Province, China under Grant No. 20192ACB21002. A.-X.C. is supported by NSFC under Grant No. 11775190. J.-Q.L. is supported in part by NSFC under Grants No. 11822501 and No. 11774087 and by Natural Science Foundation of Hunan Province, China under Grant No. 2017JJ1021.

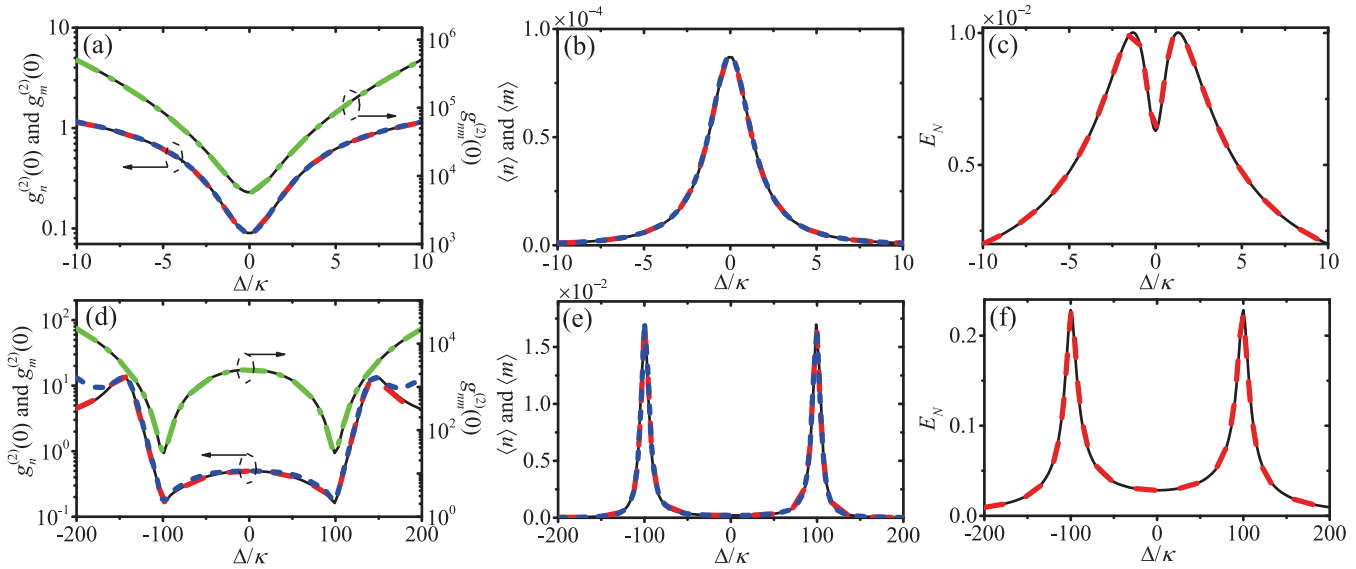

FIG. 8. In panels (a) and (d), the equal-time second-order correlation functions $[g_n^{(2)}(0)$ and $g_m^{(2)}(0)]$ and cross-correlation function $g_{nm}^{(2)}(0)$ are plotted as functions of the detuning Δ/κ. In panels (b) and (e), the mean photon (phonon) number $\langle n\rangle$ ($\langle m\rangle$) is plotted as a function of the detuning Δ/κ. In panels (c) and (f), the logarithmic negativity E_N is plotted as a function of the detuning Δ/κ. The black solid curves are obtained by the effective Hamiltonian in Eq. (5), and the other curves (red dashed, blue dotted, and green dash-dotted curves) are obtained by the Hamiltonian in Eq. (1). We set $J = 0.1\kappa$ (or $g_{ac} = 10^2\kappa$ and $g_{am} = 10^3\kappa$) in panels (a) and (b) and set $J = 100\kappa$ (or $g_{ac} = 10^3\kappa$ and $g_{am} = 10^5\kappa$) in panels (d)–(f). Other used parameters are $\gamma_c = \gamma_m = 10\kappa$, $\Omega = \kappa$, $\omega_m = 10^6\kappa$, and $m_{\rm th} = 0$.

APPENDIX: THE VALIDITY OF THE EFFECTIVE HAMILTONIAN IN EQ. (5)

In this Appendix, we will check the validity of the effective Hamiltonian in Eq. (5) numerically. As an example, Fig. 2 is replotted by using the Hamiltonian in Eq. (1) as shown in Fig. 8. In comparison, the results obtained by the effective Hamiltonian in Eq. (5) are also shown in Fig. 8 (black solid curves). The results (black solid curves) corresponding to the effective Hamiltonian in Eq. (5) agree well with the ones based on the Hamiltonian in Eq. (1) (red dashed, blue dotted, and green dash-dotted curves). It is important to emphasize that the effective Hamiltonian in Eq. (5) is valid under the conditions $\omega_0' = \omega_c + \omega_m$ and $\omega_p \approx \omega_0' \gg \{\omega_c, \omega_m\} \gg \{g_{ac}, g_{am}\} \gg \Omega$.

[1] M. Aspelmeyer, T. J. Kippenberg, and F. Marquardt, Cavity optomechanics, Rev. Mod. Phys. **86**, 1391 (2014).

[2] A. Imamoğlu, H. Schmidt, G. Woods, and M. Deutsch, Strongly Interacting Photons in a Nonlinear Cavity, Phys. Rev. Lett. **79**, 1467 (1997).

[3] K. M. Birnbaum, A. Boca, R. Miller, A. D. Boozer, T. E. Northup, and H. J. Kimble, Photon blockade in an optical cavity with one trapped atom, Nature (London) **436**, 87 (2005).

[4] Y. X. Liu, A. Miranowicz, Y. B. Gao, J. Bajer, C. P. Sun, and F. Nori, Qubit-induced phonon blockade as a signature of quantum behavior in nanomechanical resonators, Phys. Rev. A **82**, 032101 (2010).

[5] P. Rabl, Photon Blockade Effect in Optomechanical Systems, Phys. Rev. Lett. **107**, 063601 (2011).

[6] A. Nunnenkamp, K. Børkje, and S. M. Girvin, Single-Photon Optomechanics, Phys. Rev. Lett. **107**, 063602 (2011).

[7] K. Stannigel, P. Komar, S. J. M. Habraken, S. D. Bennett, M. D. Lukin, P. Zoller, and P. Rabl, Optomechanical Quantum Information Processing with Photons and Phonons, Phys. Rev. Lett. **109**, 013603 (2012).

[8] A. Kronwald, M. Ludwig, and F. Marquardt, Full photon statistics of a light beam transmitted through an optomechanical system, Phys. Rev. A **87**, 013847 (2013).

[9] X. W. Xu, Y. J. Li, and Y. X. Liu, Photon-induced tunneling in optomechanical systems, Phys. Rev. A **87**, 025803 (2013).

[10] J. Q. Liao and F. Nori, Photon blockade in quadratically coupled optomechanical systems, Phys. Rev. A **88**, 023853 (2013).

[11] X. Y. Lü, Y. Wu, J. R. Johansson, H. Jing, J. Zhang, and F. Nori, Squeezed Optomechanics with Phase-Matched Amplification and Dissipation, Phys. Rev. Lett. **114**, 093602 (2015).

[12] D. Hu, S. Y. Huang, J. Q. Liao, L. Tian, and H. S. Goan, Quantum coherence in ultrastrong optomechanics, Phys. Rev. A **91**, 013812 (2015).

[13] H. Xie, G. W. Lin, X. Chen, Z. H. Chen, and X. M. Lin, Single-photon nonlinearities in a strongly driven optomechanical system with quadratic coupling, Phys. Rev. A **93**, 063860 (2016).

[14] H. Seok and E. M. Wright, Antibunching in an optomechanical oscillator, Phys. Rev. A **95**, 053844 (2017).

[15] H. Xie, C. G. Liao, X. Shang, M. Y. Ye, and X. M. Lin, Phonon blockade in a quadratically coupled optomechanical system, Phys. Rev. A **96**, 013861 (2017).

[16] X. W. Xu and Y. J. Li, Antibunching photons in a cavity coupled to an optomechanical system, J. Phys. B **46**, 035502 (2013).
[17] V. Savona, Unconventional photon blockade in coupled optomechanical systems, arXiv:1302.5937.
[18] H. Q. Shi, X. T. Zhou, X. W. Xu, and N. H. Liu, Tunable phonon blockade in quadratically coupled optomechanical systems, Sci. Rep. **8**, 2212 (2018).
[19] M. Wang, X.-Y. Lü, A. Miranowicz, T.-S. Yin, Y. Wu, and F. Nori, Unconventional phonon blockade via atom-photon-phonon interaction in hybrid optomechanical systems, arXiv:1806.03754.
[20] B. Li, R. Huang, X. W. Xu, A. Miranowicz, and H. Jing, Nonreciprocal unconventional photon blockade in a spinning optomechanical system, Photon. Res. **7**, 630 (2019).
[21] R. Riedinger, S. Hong, R. A. Norte, J. A. Slater, J. Shang, A. G. Krause, V. Anant, M. Aspelmeyer, and S. Gröblacher, Non-classical correlations between single photons and phonons from a mechanical oscillator, Nature (London) **530**, 313 (2016).
[22] S. Carlig and M. A. Macovei, Quantum correlations among optical and vibrational quanta, Phys. Rev. A **89**, 053803 (2014).
[23] X. W. Xu, H. Q. Shi, A. X. Chen, and Y. X. Liu, Cross-correlation between photons and phonons in quadratically coupled optomechanical systems, Phys. Rev. A **98**, 013821 (2018).
[24] D. Vitali, S. Gigan, A. Ferreira, H. R. Böhm, P. Tombesi, A. Guerreiro, V. Vedral, A. Zeilinger, and M. Aspelmeyer, Optomechanical Entanglement between a Movable Mirror and a Cavity Field, Phys. Rev. Lett. **98**, 030405 (2007).
[25] M. J. Hartmann and M. B. Plenio, Steady State Entanglement in the Mechanical Vibrations of Two Dielectric Membranes, Phys. Rev. Lett. **101**, 200503 (2008).
[26] K. Børkje, A. Nunnenkamp, and S. M. Girvin, Proposal for Entangling Remote Micromechanical Oscillators via Optical Measurements, Phys. Rev. Lett. **107**, 123601 (2011).
[27] Sh. Barzanjeh, M. Abdi, G. J. Milburn, P. Tombesi, and D. Vitali, Reversible Optical-to-Microwave Quantum Interface, Phys. Rev. Lett. **109**, 130503 (2012).
[28] Y. D. Wang and A. A. Clerk, Using Interference for High Fidelity Quantum State Transfer in Optomechanics, Phys. Rev. Lett. **108**, 153603 (2012).
[29] L. Tian, Adiabatic State Conversion and Pulse Transmission in Optomechanical Systems, Phys. Rev. Lett. **108**, 153604 (2012).
[30] T. A. Palomaki, J. D. Teufel, R. W. Simmonds, and K. W. Lehnert, Entangling Mechanical Motion with Microwave Fields, Science **342**, 710 (2013).
[31] R. Riedinger, A. Wallucks, I. Marinković, C. Löschnauer, M. Aspelmeyer, S. Hong, and S. Gröblacher, Remote quantum entanglement between two micromechanical oscillators, Nature (London) **556**, 473 (2018).
[32] C. F. Ockeloen-Korppi, E. Damskägg, J.-M. Pirkkalainen, M. Asjad, A. A. Clerk, F. Massel, M. J. Woolley, and M. A. Sillanpää, Stabilized entanglement of massive mechanical oscillators, Nature (London) **556**, 478 (2018).
[33] I. Marinković, A. Wallucks, R. Riedinger, S. Hong, M. Aspelmeyer, and S. Gröblacher, Optomechanical Bell Test, Phys. Rev. Lett. **121**, 220404 (2018).
[34] W. J. Nie, Y. H. Lan, Y. Li, and S. Y. Zhu, Effect of the Casimir force on the entanglement between a levitated nanosphere and cavity modes, Phys. Rev. A **86**, 063809 (2012).
[35] X. W. Xu, Y. J. Zhao, and Y. X. Liu, Entangled-state engineering of vibrational modes in a multimembrane optomechanical system, Phys. Rev. A **88**, 022325 (2013).
[36] J. Q. Liao, Q. Q. Wu, and F. Nori, Entangling two macroscopic mechanical mirrors in a two-cavity optomechanical system, Phys. Rev. A **89**, 014302 (2014).
[37] X. Y. Lü, G. L. Zhu, L. L. Zheng, and Y. Wu, Entanglement and quantum superposition induced by a single photon, Phys. Rev. A **97**, 033807 (2018).
[38] M. Paternostro, D. Vitali, S. Gigan, M. S. Kim, C. Brukner, J. Eisert, and M. Aspelmeyer, Creating and Probing Multipartite Macroscopic Entanglement with Light, Phys. Rev. Lett. **99**, 250401 (2007).
[39] C. Genes, A. Mari, P. Tombesi, and D. Vitali, Robust entanglement of a micromechanical resonator with output optical fields, Phys. Rev. A **78**, 032316 (2008).
[40] H. T. Tan and G. X. Li, Multicolor quadripartite entanglement from an optomechanical cavity, Phys. Rev. A **84**, 024301 (2011).
[41] A. Xuereb, M. Barbieri, and M. Paternostro, Multipartite optomechanical entanglement from competing nonlinearities, Phys. Rev. A **86**, 013809 (2012).
[42] J. Li, S. Y. Zhu, and G. S. Agarwal, Magnon-Photon-Phonon Entanglement in Cavity Magnomechanics, Phys. Rev. Lett. **121**, 203601 (2018).
[43] J.-M. Pirkkalainen, S. U. Cho, F. Massel, J. Tuorila, T. T. Heikkila, P. J. Hakonen, and M. A. Sillanpää, Cavity optomechanics mediated by a quantum two-level system, Nat. Commun. **6**, 6981 (2015).
[44] Y. Chang, H. Ian, and C. P. Sun, Triple coupling and parameter resonance in quantum optomechanics with a single atom, J. Phys. B **42**, 215502 (2009).
[45] M. Cotrufo, A. Fiore, and E. Verhagen, Coherent Atom-Phonon Interaction through Mode Field Coupling in Hybrid Optomechanical Systems, Phys. Rev. Lett. **118**, 133603 (2017).
[46] T. T. Heikkila, F. Massel, J. Tuorila, R. Khan, and M. A. Sillanpää, Enhancing Optomechanical Coupling via the Josephson Effect, Phys. Rev. Lett. **112**, 203603 (2014).
[47] F. Tian, H. Sumikura, E. Kuramochi, M. Takiguchi, M. Ono, A. Shinya, and M. Notomi, All-optical dynamic modulation of spontaneous emission rate in hybrid optomechanical cavity quantum electrodynamics systems, arXiv:1901.07691.
[48] J. D. Teufel, D. Li, M. S. Allman, K. Cicak, A. J. Sirois, J. D. Whittaker, and R. W. Simmonds, Circuit cavity electromechanics in the strong-coupling regime, Nature (London) **471**, 204 (2011).
[49] F. Massel, S. Un Cho, J.-M. Pirkkalainen, P. J. Hakonen, T. T. Heikkilä, and M. A. Sillanpää, Multimode circuit optomechanics near the quantum limit, Nat. Commun. **3**, 987 (2012).
[50] J. Suh, A. J. Weinstein, C. U. Lei, E. E. Wollman, S. K. Steinke, P. Meystre, A. A. Clerk, and K. C. Schwab, Mechanically detecting and avoiding the quantum fluctuations of a microwave field, Science **344**, 1262 (2014).
[51] J. D. Thompson, B. M. Zwickl, A. M. Jayich, F. Marquardt, S. M. Girvin, and J. G. E. Harris, Strong dispersive coupling of a high-finesse cavity to a micromechanical membrane, Nature (London) **452**, 72 (2008).

[52] N. E. Flowers-Jacobs, S. W. Hoch, J. C. Sankey, A. Kashkanova, A. M. Jayich, C. Deutsch, J. Reichel, and J. G. E. Harris, Fiber-cavity-based optomechanical device, Appl. Phys. Lett. **101**, 221109 (2012).

[53] H. Xu, D. Mason, L. Jiang, and J. G. E. Harris, Topological energy transfer in an optomechanical system with exceptional points, Nature (London) **537**, 80 (2016).

[54] H. Xu, U. Kemiktarak, J. Fan, S. Ragole, J. Lawall, and J. M. Taylor, Observation of optomechanical buckling transitions, Nat. Commun. **8**, 14481 (2017).

[55] H. J. Carmichael, *An Open Systems Approach to Quantum Optics*, Lecture Notes in Physics Vol. 18 (Springer-Verlag, Berlin, 1993).

[56] G. Vidal and R. F. Werner, Computable measure of entanglement, Phys. Rev. A **65**, 032314 (2002).

[57] G. Adesso, A. Serafini, and F. Illuminati, Extremal entanglement and mixedness in continuous variable systems, Phys. Rev. A **70**, 022318 (2004).

[58] S. E. Harris, Electromagnetically induced transparency, Phys. Today **50**(7), 36 (1997).

[59] M. Fleischhauer, A. Imamoglu, and J. P. Marangos, Electromagnetically induced transparency: Optics in coherent media, Rev. Mod. Phys. **77**, 633 (2005).

[60] G. S. Agarwal and S. Huang, Electromagnetically induced transparency in mechanical effects of light, Phys. Rev. A **81**, 041803(R) (2010).

[61] S. Weis, R. Riviere, S. Deleglise, E. Gavartin, O. Arcizet, A. Schliesser, and T. J. Kippenberg, Optomechanically induced transparency, Science **330**, 1520 (2010).

[62] A. H. Safavi-Naeini, T. P. Mayer Alegre, J. Chan, M. Eichenfield, M. Winger, Q. Lin, J. T. Hill, D. E. Chang, and O. Painter, Electromagnetically induced transparency and slow light with optomechanics, Nature (London) **472**, 69 (2011).

[63] I. Wilson-Rae, N. Nooshi, W. Zwerger, and T. J. Kippenberg, Theory of Ground State Cooling of a Mechanical Oscillator Using Dynamical Backaction, Phys. Rev. Lett. **99**, 093901 (2007).

[64] F. Marquardt, J. P. Chen, A. A. Clerk, and S. M. Girvin, Quantum Theory of Cavity-Assisted Sideband Cooling of Mechanical Motion, Phys. Rev. Lett. **99**, 093902 (2007).

[65] Y. Li, Y. D. Wang, F. Xue, and C. Bruder, Quantum theory of transmission line resonator-assisted cooling of a micromechanical resonator, Phys. Rev. B **78**, 134301 (2008).

[66] X. W. Xu, Y. X. Liu, C. P. Sun, and Y. Li, Mechanical $\mathcal{PT}$ symmetry in coupled optomechanical systems, Phys. Rev. A **92**, 013852 (2015).

[67] N. Didier, S. Pugnetti, Y. M. Blanter, and R. Fazio, Detecting phonon blockade with photons, Phys. Rev. B **84**, 054503 (2011).

[68] T. Ramos, V. Sudhir, K. Stannigel, P. Zoller, and T. J. Kippenberg, Nonlinear Quantum Optomechanics via Individual Intrinsic Two-Level Defects, Phys. Rev. Lett. **110**, 193602 (2013).

[69] J. D. Cohen, S. M. Meenehan, G. S. MacCabe, S. Groblacher, A. H. Safavi-Naeini, F. Marsili, M. D. Shaw, and O. Painter, Phonon counting and intensity interferometry of a nanomechanical resonator, Nature (London) **520**, 522 (2015).

[70] X. W. Xu, A. X. Chen, and Y. X. Liu, Phonon blockade in a nanomechanical resonator resonantly coupled to a qubit, Phys. Rev. A **94**, 063853 (2016).

[71] A. D. O'Connell, M. Hofheinz, M. Ansmann, R. C. Bialczak, M. Lenander, E. Lucero, M. Neeley, D. Sank, H. Wang, M. Weides, J. Wenner, J. M. Martinis, and A. N. Cleland, Quantum ground state and single-phonon control of a mechanical resonator, Nature (London) **464**, 697 (2010).

[72] S. C. Gou, Quantum behavior of a two-level atom interacting with two modes of light in a cavity, Phys. Rev. A **40**, 5116 (1989).

[73] M. M. Ashraf and M. S. K. Razmi, Atomic-dipole squeezing and emission spectra of the nondegenerate two-photon Jaynes-Cummings model, Phys. Rev. A **45**, 8121 (1992).

[74] C. Zhong, Z. Wang, C. Zou, M. Zhang, X. Han, W. Fu, M. Xu, S. Shankar, M. H. Devoret, H. X. Tang, and L. Jiang, Heralded generation and detection of entangled microwave-optical photon pairs, arXiv:1901.08228.